JOURNAL OF COMPUTATIONAL PHYSICS 40, 396–410 (1981)

Interactive Method for Computation of Viscous Flow with Recirculation

JULIUS BRANDEIS* AND JOSEF ROM†

Department of Aeronautical Engineering, Technion—Israel Institute of Technology, Haifa, Israel

Received May 1, 1980

An interactive method is proposed for the solution of two-dimensional, laminar flow fields with identifiable regions of recirculation, such as the shear layer driven cavity flow. The method treats the flow field as composed of two regions, with an appropriate mathematical model adopted for each region. The shear layer is computed by the compressible boundary layer equations, and the slowly recirculating flow by the incompressible Navier–Stokes equations. The flow field is solved iteratively by matching the local solutions in the two regions. For this purpose a new matching method utilizing an overlap between the two computational regions is developed, and shown to be most satisfactory. Matching of u, v, as well as $\partial u/\partial y$ is amply accomplished using the present approach, and the stagnation points corresponding to separation and reattachment of the dividing streamline are computed as part of the interactive solution. The interactive method is applied to the test problem of shear layer driven cavity. The computational results are used to show the validity and applicability of the present approach.

INTRODUCTION

This paper proposes a new interactive two-layer method for computation of two-dimensional flow fields consisting of shear layer flowing over a region with significant recirculation. Such flows are typically characterized by transition between a high speed, compressible outer layer and a region containing fluid in slow, recirculatory motion. To compute a solution to such flow field one may apply the most general mathematical model valid in the whole region, usually the set of compressible Navier–Stokes equations. Alternatively, a simplified, zonal model may be used.

The interactive approach presented in this paper is based on dividing the flow field into two regions, in each of which an appropriate mathematical model is used. Thus, the parabolic boundary layer equations of compressible, laminar flow are to be solved in the boundary layer/shear layer region. This region is assumed to be thin in order for the boundary layer approximation to be valid.

Within the region of reversed flow, the elliptic, incompressible Navier–Stokes equations are used. These constitute a valid model for the slowly recirculating flow

* Graduate Instructor, presently an NRC Associate at NASA–Ames Research Center Moffett Field, California 94035.

† Professor, Lady David Chair in Experimental Aerodynamics.

0021-9991/81/040396–15$02.00/0

encountered there, capable of dealing with stagnation points encountered at separation and reattachment of the diving streamline.

The continuity of solution must be assured between the two regions by matching the flow variables at the interface. For this purpose, a new matching model, making use of partial overlap between the two computational regions is developed. As will be shown, the overlap facilitates matching not only of the two velocity components, but of $\partial u/\partial y$ as well. Furthermore, the present model allows the use of the second order–accurate central difference scheme for updating the boundary conditions, as these are always computed at internal points of the adjoining region. Consequently, no assumptions need to be made concerning the dividing streamline, which, together with its stagnation points, emerges naturally from the solution.

The interactive approach offers several advantages over the methods employing the general Navier–Stokes equations for solution of the total flow field. For instance, using the parabolic boundary layer equations, the limitations on the field size and cell Reynolds number are avoided in the shear layer, and no need exists for assuming the outflow boundary conditions. Furthermore, the interactive methods in general require significantly smaller computer processing time as well as core space, making their use economically preferable.

The interactive model developed in this paper is applied to the problem of shear layer driven cavity flows in which the free stream is supersonic. The simplicity of geometry as well as its relevance to various aerodynamic problems make cavity a suitable test configuration for the present model (Fig. 1). The computational results are used to show validity and merits of the present approach as a method for computation of flow fields with significant recirculation.

Although the cavity geometry is a standard test case used for validation of methods, few works were found in literature addressing the problem of the shear layer driven cavity. Briefly, Mehta and Lavan [6] and O'Brien [7] obtained Navier–Stokes solutions to the flow field in a channel containing a cavity in the lower wall. Weiss and Florsheim [11] developed a simplified model for the shear layer driven cavity flow based on assuming a straight dividing streamline having its stagnation points at

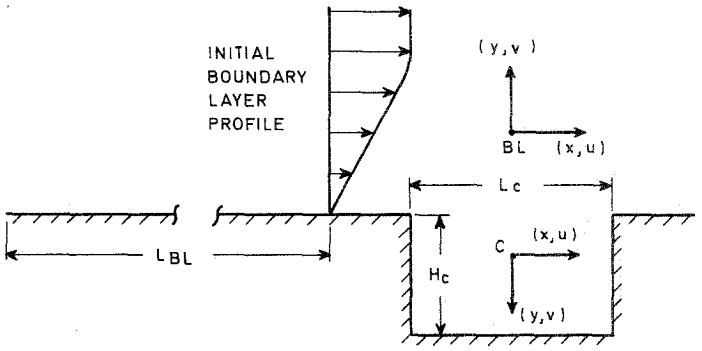

FIG. 1. Geometry and coordinate systems for the interactive shear layer–cavity calculation.

the two convex corners. As will be shown, the present method is free from such restrictions. A thorough experimental treatment of the flow inside rectangular cavities was presented by Charwat *et al.* [4, 5]. This work also shows some indications of periodicity in cavity flows, which was recently the subject of numerical study by Borland [1], who used an inviscid flow model for this purpose. This unsteady behavior of the cavity flows is indicated in a growing number of experimental works, focusing on the acoustic aspect of the problem.

However, if the unsteadiness is dynamically weak in comparison with the supersonic free stream, the mean geometrical characteristics of the cavity may not be strongly influenced by the internal structure of the flow. For this reason, steady analyses of base flows are successful in predicting the base pressure. Likewise, the present model focusing on the interaction of the shear layer with the recirculating cavity flow will be restricted to the steady state. Since the problem of joint solution for mathematically parabolic and elliptic regions is considered, a constraint of zero streamwise pressure gradient will be imposed in the test cases. The interaction with the outer flow, using the present approach, has been shown to be feasible by Brandeis [2].

Mathematical Formulation of the Flow in the Two Layers

For the shear layer, the governing equations of the compressible, laminar boundary layer, non-dimensionalized by the free stream reference quantities are

Momentum

$$\rho u \frac{\partial u}{\partial x} + \rho v \frac{\partial u}{\partial y} = -\frac{dp}{dx} + \frac{1}{Re} \frac{\partial}{\partial y}\left(\mu \frac{\partial u}{\partial y}\right), \tag{1}$$

Energy

$$\rho u \frac{\partial T}{\partial x} + \rho v \frac{\partial T}{\partial y} = u \frac{dp}{dx} + \frac{1}{Re\,Pr} \frac{\partial}{\partial y}\left(\mu \frac{\partial T}{\partial y}\right) + \frac{\mu}{Re}\left(\frac{\partial u}{\partial y}\right)^2, \tag{2}$$

Continuity

$$\frac{\partial(\rho u)}{\partial x} + \frac{\partial(\rho v)}{\partial y} = 0. \tag{3}$$

In addition, the equation of state and the viscosity relation are defined, respectively, as

$$p = \frac{\gamma - 1}{\gamma} \rho T, \tag{4}$$

$$\mu = [(\gamma - 1) M_0^2]^{0.76} T^{0.76}. \tag{5}$$

Equation (5) arises from the power law relation for viscosity, in which the temperature ratio is raised to the power 0.76 after Chapman [3].

The boundary conditions along the outer edge of the viscous layer are found from the following relations compatible with the external flow

$$\rho_e u_e \frac{\partial u_e}{\partial x} = -\frac{dp}{dx} \; (\equiv 0), \tag{6}$$

$$\rho_e u_e \frac{\partial T_e}{\partial x} = -u_e \frac{dp}{dx} \; (\equiv 0), \tag{7}$$

while the conditions on u and v along the interface with the cavity are obtained through matching, with adiabatic "surface" ($\partial T/\partial y = 0$) assumed along the line joining the two convex corners of the cavity (CD in Fig. 2). This line, along which the boundary conditions for the shear layer are specified, was found, for the cases considered, to be not far removed from the dividing streamline.

The system of equations (1)–(5) together with the boundary conditions is solved downstream of the initial station. The computational region is taken to extend in the lateral direction high enough so that the velocity and temperature gradients $\partial u/\partial y$ and $\partial T/\partial y$ can be neglected at the outer boundary.

The numerical solution in the viscous layer is obtained by replacing the nonlinear partial differential equations with a set of linear difference equations, as done by Reyhner *et al.* [8]. The solution obtained at each step from the linear difference equations is used to calculate an improved solution at that step through iteration, until the differences between flow variables for two successive iterations are as small as desired.

The recirculating flow is contained in the present case by a rectangular cavity bounded on three sides by no-slip walls. Along the fourth, open boundary, the flow merges with the shear layer which through the action of viscous stresses provides the driving force for the recirculation. For small cavities ($L \sim H \sim O(\delta)$) the anticipated recirculation velocities are in the low subsonic range even for moderate supersonic

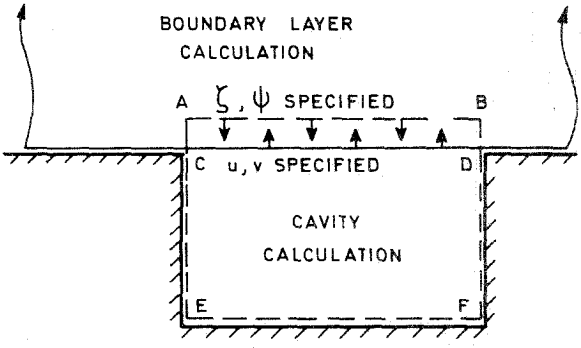

FIG. 2. Schematic of the overlapping regions used for matching

Mach numbers in the outer flow. Consequently, computation of the cavity flow is carried out with the incompressible Navier–Stokes equations. As a further consequence of the low recirculation velocities, the density and velocity fields are assumed to be only weakly coupled, and the energy equation is not considered at the present stage. The fluid within the cavity is thus assumed to be in thermal equilibrium with the wall, allowing the adiabatic boundary condition to be used at the interphase for the shear layer. The energy equation could be included iteratively in the present recirculating flow model if the particular problem required this. In such case, an additional matching condition, relating to temperature, would have to be imposed.

Incompressible Navier–Stokes equations written in the vorticity–stream function form and normalized by cavity length (L_c), typical velocity (U_c) and characteristic density and viscosity, are

$$\frac{\partial \zeta}{\partial t} = -u\frac{\partial \zeta}{\partial x} - v\frac{\partial \zeta}{\partial y} + \frac{1}{Re}\nabla^2\zeta, \tag{8}$$

$$\frac{\partial \psi}{\partial t'} = \nabla^2\psi - \zeta. \tag{9}$$

t' in Eq. (9) can be regarded as a non-physical iteration time. Only the converged result (steady state) is of interest. The boundary conditions at the three no-slip walls are

$$\psi = 0,$$
$$\zeta = \partial^2\psi/\partial y^2 \qquad \text{along horizontal wall,}$$
$$\zeta = \partial^2\psi/\partial x^2 \qquad \text{along vertical walls.}$$

ψ and ζ along the fluid interface boundary are determined by matching and will be discussed later, together with the matching method.

Equations (8) and (9) are discretized using the fully explicit, second order accurate Forward Time–Center Space (FTCS) numerical scheme. The finite difference equations are obtained, in their conservative form, by directly substituting the appropriate expressions for the first and second order derivatives which are of the form

$$\frac{\partial f}{\partial x} = \frac{f_{i+1,j} - f_{i-1,j}}{2\Delta x},$$

$$\frac{\partial^2 f}{\partial x^2} = \frac{f_{i+1,j} + f_{i-1,j} - 2f_{i,j}}{(\Delta x)^2}$$

into the governing equations (8) and (9). Similar expressions are obtained for $\partial f/\partial y$ and $\partial^2 f/\partial y^2$. ($f$ represents the dependent variables.)

The boundary condition for ζ at the horizontal wall is discretized by writing the Taylor series expansion for ψ at the first grid point away from the wall

$$\psi_{\Delta y} = \psi_w + \frac{\partial \psi}{\partial y}\bigg|_w \Delta y + \frac{1}{2}\frac{\partial^2 \psi}{\partial y^2}\bigg|_w (\Delta y)^2 + O((\Delta y)^2)$$

then noting that $\partial\psi/\partial y|_w = 0$ and substituting the result into the boundary condition to give

$$\zeta_w = \frac{2(\psi_{\Delta y} - \psi_w)}{(\Delta y)^2}.$$

Similar results are obtained for vertical walls.

The convex corners, which are singular points in both the boundary layer and the Navier–Stokes formulations, did not present a problem in the numerical solutions used in the two regions. The solution for the shear layer was confined to the region above the line joining the two corners and thus it was sufficient to specify $u = v = 0$ at those two points. For the Navier–Stokes solution, the physical corners (C and D in Fig. 2) were assigned the values of vorticity found from the no slip condition $\zeta = \partial^2\psi/\partial y^2$, as for all other points along the wall. The "corners" of the computational region (A and B in Fig. 2) also presented no difficulty, as the vorticity there was uniquely determined from the shear layer solution.

Although the Reynolds number limit for stability associated with the present approach, is only somewhat higher than 100, it proved sufficiently high for the modest size cavities considered in this study.

Shear Layer–Recirculating Flow Interaction

The equations of motion for the shear layer (Eqs. (1)–(5)) and for the recirculating flow (Eqs. (8), (9)) are to be solved under the constraints imposed by matching.

It is recalled that in formulation of the mathematical models for the shear layer and for the recirculating flow, two different sets of normalization factors were used. Consequently, two different scales are inherent in the interaction, involving two different Reynolds numbers:

$$Re_{BL} = \frac{\rho_{BL} U_{BL} L_{BL}}{\mu_{BL}} \qquad \text{for the shear layer}$$

and

$$Re_c = \frac{\rho_c U_c L_c}{\mu_c} \qquad \text{for the cavity}$$

(multiple scale approach for interactive solutions has been discussed by Rom [10]).

The geometry of the matching model adopted in this work is illustrated in Fig. 2. The important, innovative feature of this model is the presence of the overlap region *ABCD* between the domains of shear layer and recirculating flow computation. There are now seen to be two matching boundaries, *AB* and *CD*, defining the matching region in which the solution undergoes "transition" between the two fields of computation.

The upper matching line, *AB*, is contained within the region where flow is calculated by the boundary layer equations. It is also the upper boundary for the Navier–Stokes calculation of the cavity flow inside the rectangle *ABFE*. Vorticity, ζ, and stream function, ψ, are then calculated within the shear layer using

$$\zeta = \frac{\partial u}{\partial y} - \frac{\partial v}{\partial x}, \tag{10}$$

$$\frac{\partial^2 \psi}{\partial x^2} = -\frac{\partial v}{\partial x}. \tag{11}$$

All derivatives in the right-hand side of Eqs. (10) and (11) were computed from the shear layer using the second order–accurate central differences. ψ is then obtained by numerical integration along the boundary of the following equivalent of Eq. (11)

$$\psi_{i+1,j} - 2\psi_{i,j} + \psi_{i-1,j} = -\frac{\partial v}{\partial x}(\Delta x)^2.$$

The integration is accomplished using the tri-diagonal procedure. The values of ψ at the two end points are easily obtained from the boundary layer solution.

The lower matching line, *CD*, is analogously seen to lie within the Navier–Stokes computation region, from which, then, the velocities u and v are calculated and supplied as boundary conditions for the shear layer computation. The condition on u is specified at each grid point, while that on v is imposed at the mid-points between the nodes. This distribution of boundary conditions resulted in improved convergence characteristics of the solution when compared to computations in which u and v were both prescribed at the node points.

Each time that boundary conditions are exchanged between the regions, their scaling has to be adjusted accordingly.

The height of the overlap region is taken here as one grid interval in the transverse direction, though it need not be restricted as such. One criterion to be considered in adjusting the height of the overlap region is the validity of the incompressibility assumption for the flow within the cavity.

It is noteworthy, that the present method does not require any assumption concerning the location of the stagnation points. These are obtained from the results of the calculation as part of the iterative solution. The location of stagnation points corresponds to the points of zero vorticity on the walls (i.e., where wall vorticity undergoes a change in sign).

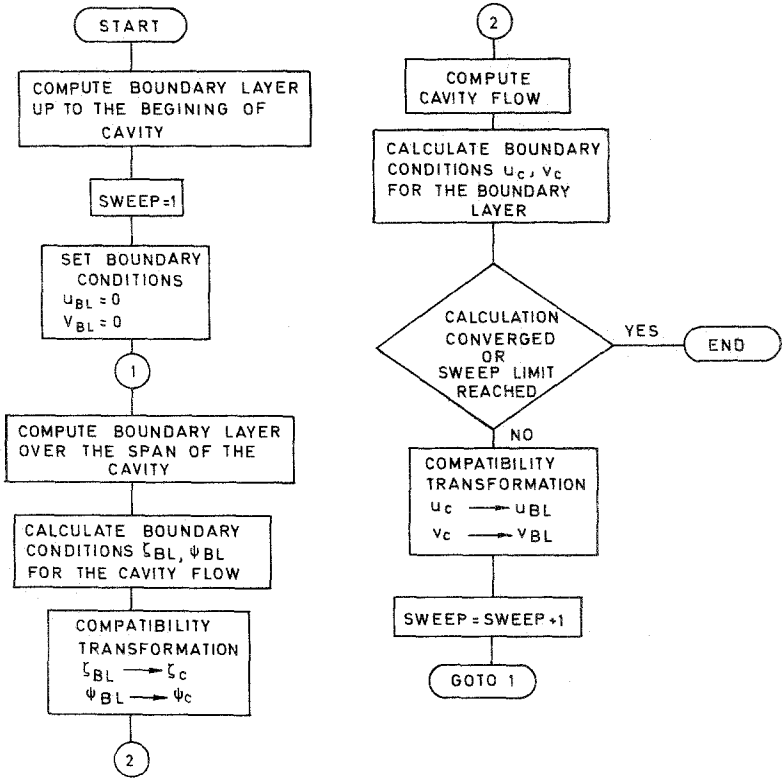

FIG. 3. Flow diagram for the interactive shear layer–cavity calculation.

The interactive computation of the shear layer and the recirculating flow is carried out through iteration. Flow diagram for the procedure is presented in Fig. 3. Initially, the boundary layer calculation is advanced to the beginning of the cavity region. Then for the first iteration, called sweep, the shear layer is computed over the span of the cavity until its end, under the familiar boundary layer conditions $u = v = 0$. The necessary calculations of ζ and ψ are made and these undergo the compatibility transformation before being supplied to the cavity region as boundary conditions.

The cycle is continued with the calculation of the recirculating flow, and, consequently, of the new set of boundary conditions for the shear layer, thus completing the first sweep. For subsequent sweeps, the shear layer calculation is initiated at the beginning of the cavity region. This iterative process is continued until the maximum difference between flow variables at two successive iterations is acceptably small. For the present purpose the interactive computation was stopped after the 20th sweep, at which point convergence was checked.

The following expression was used for calculating the convergence error:

$$(\varepsilon_f)_{\text{Max}} = \left.\frac{f_{sw} - f_{sw-1}}{(f_{\text{Max}})_{sw}}\right]_{\text{Max}}, \tag{12}$$

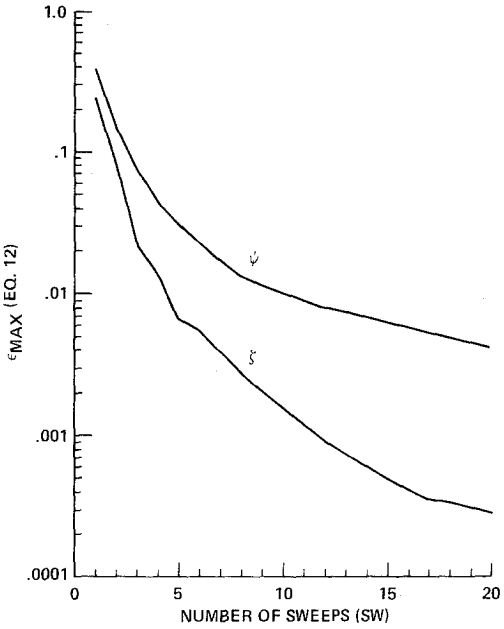

FIG. 4. Convergence characteristics for the shear layer–cavity calculation. $AR = 0.4$, 11×12 grid points, $Re_c = 5.4$, $Re_{BL} = 10^5$.

where f refers to the particular variable under scrutiny, and sw is the sweep number. The variation of the maximum error with the sweep number for the first 20 sweeps was calculated using Eq. (12) and the results are plotted in Fig. 4 for the cavity of $AR = 0.4$. These results, which are typical of all aspects ratios considered, indicate that convergence to within 1% accuracy for both ζ and ψ is obtained after the first ten sweeps. The stream function typically was slower in convergence compared to vorticity for all shear layer cavity flows computed, though the difference appears to diminish when the solution is allowed to proceed past the first 20 sweeps shown in Fig. 4. Interestingly, both variables showed similar convergence rates when a flow-through boundary was substituted for the lower wall of the cavity (EF in Fig. 2), indicating that the specific geometry rather than the method is responsible for the unequal convergence of ψ and ζ.

APPLICATION OF METHOD AND RESULTS

The results of applying the interactive method to the shear layer driven cavity flows whose geometry is illustrated in Fig. 1, are now presented. Configurations with cavities of several aspects ratios ($AR = H_c/L_c$ = depth/span) ranging from 0.4 to 3.0 were computed with the boundary layer Reynolds number of 10^5 and 4×10^5. The

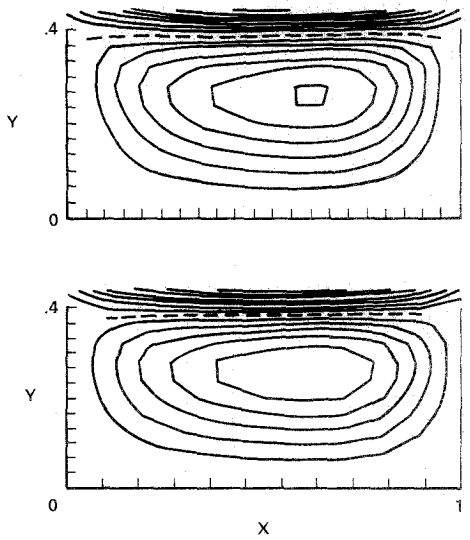

FIG. 5. Stream function contour maps for the interactive shear layer–cavity solution: $\mathcal{R} = 0.4$, $Re_c = 5.4$, $Re_{BL} = 10^5$, $Pr = 1$, $M_\infty = 2.25$, computed with two grid sizes: top—$\Delta X = 5 \times 10^{-4}$, $\Delta Y = 4 \times 10^{-4}$; bottom—$\Delta X = 10^{-3}$, $\Delta Y = 4 \times 10^{-4}$.

Reynolds number in the cavities considered varied between 5 and 21. For most cases considered, the non-dimensional boundary layer step size, Δx, was 10^{-3} and grid spacing in the lateral direction, Δy, was 4×10^{-4}. The external stream Mach number was 2.25. The grid spacing for the cavity in both x and y directions was equal to the corresponding value for the boundary layer computation, when compared in the physical space. The lateral grid spacing used for the cavity flow computation was considered to be sufficiently fine since small cavities with $H_c \simeq L_c \simeq O(\delta)$ were

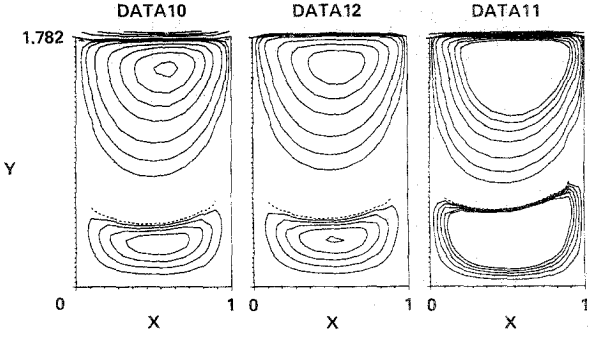

FIG. 6. Stream function contour maps for cavity: $\mathcal{R} = 2.0$, $Re_c = 5.4$, $Re_{BL} = 10^5$, $Pr = 1$, $M_\infty = 2.25$. left—shear layer driven, middle—wall driven, inflow condition, right—wall driven, averaged velocity.

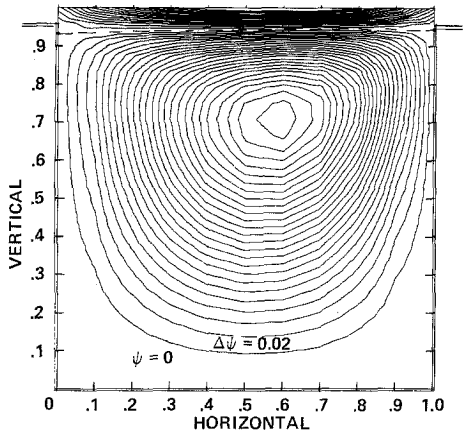

FIG. 7. Stream function contour map for the interactive shear layer–cavity solution: $\mathcal{R} = 1$, $Re_c = 5.4$, $Re_{BL} = 10^5$, $Pr = 1$, $M_\infty = 2.25$.

considered. A check was made, however, of the effect of reducing the streamwise spacing between the mesh points to see if $\Delta x = 10^{-3}$ was sufficiently small. For this purpose solutions were obtained for the configuration having $\mathcal{R} = 0.4$, $Re_{BL} = 10^5$ and $Re_c = 5.4$, with Δx of 10^{-3} and 5×10^{-4}. The resulting stream function maps are presented in Fig. 5 for comparison. The $\Delta\psi$ was kept equal for both cases.

An examination was made of the effect and importance of proper coupling between the shear layer and the recirculating flow. This was accomplished through comparison of the shear-layer drive cavity flow computed using the present method, and the same cavity flow driven by a horizontal wall in motion along the straight line defined by the segment AB in Fig. 2. The latter solution was generated by the same

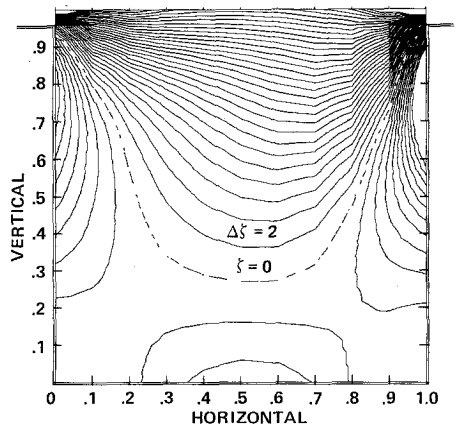

FIG. 8. Voticity contour map for the interactive shear layer–cavity solution: $\mathcal{R} = 1$, $Re_c = 5.4$, $Re_{BL} = 10^5$, $Pr = 1$, $M_\infty = 2.25$.

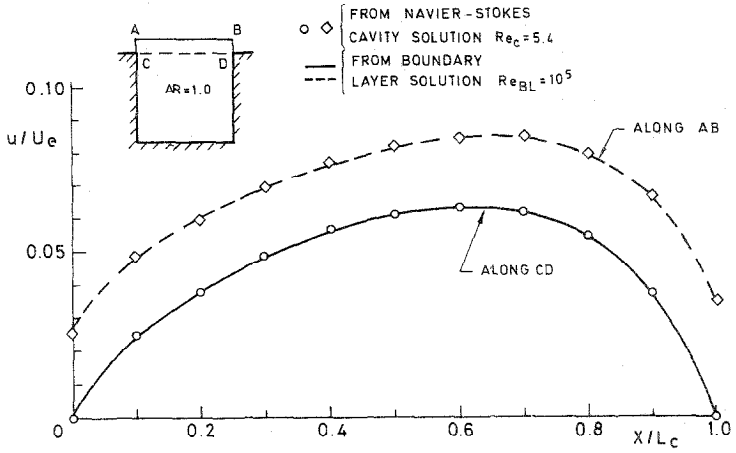

FIG. 9. Streamwise velocity component distribution along the matching boundaries for the interactive shear layer–cavity solution: $\mathcal{AR} = 1$, $Re_c = 5.4$, $Re_{BL} = 10^5$, $Pr = 1$, $M_\infty = 2.25$.

numerical model used for the shear layer driven cavity. Two definitions for the wall velocity were used: in one it was taken to be the average u along AB in Fig. 2 taken from the shear layer solution; in the other, the value of u at point A within the shear layer was adopted, which then fixes the amount of mass flowing in through the "slot" AC in Fig. 2 at the same value as computed using the interactive solution. This comparison was carried out for the deep cavity of $\mathcal{AR} = 2$ and $Re_c = 5.4$. Re_{BL} was 10^5. The resulting stream function maps are shown in Fig. 6. Data 10, 11, and 12 correspond, respectively, to the shear layer driven cavity, wall velocity computed from averaging and wall velocity taken from the point value. The streamline spacing is consistent for all three cases, but it should be noted that much smaller spacing is used for the secondary vortex in all three cases, than for the primary one.

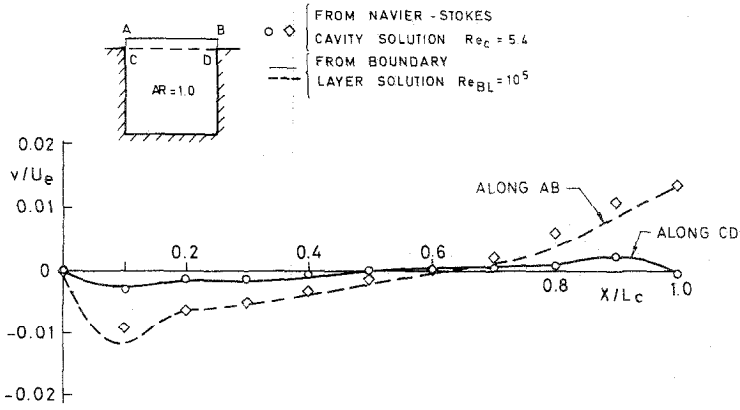

FIG. 10. Transverse velocity component distribution along the matching boundaries for the interactive shear layer–cavity solution: $\mathcal{AR} = 1$, $Re_c = 5.4$, $Re_{BL} = 10^5$, $Pr = 1$, $M_\infty = 2.25$.

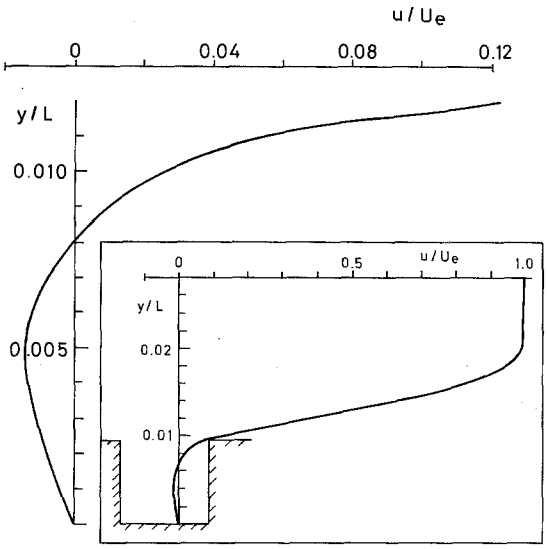

FIG. 11. Streamwise velocity profile in the recirculating flow and the shear layer, passing through the center of the vortex: $\mathcal{R} = 1$, $Re_c = 5.4$, $Re_{BL} = 10^5$, $Pr = 1$, $M_\infty = 2.25$.

Next, a set of results for a typical case of $\mathcal{R} = 1$, $Re_{BL} = 10^5$ and $Re_c = 5.4$ is presented in Figs. 7 to 10. It consists of stream function map, equal vorticity contour map, and plots of u and v velocities in the matching region, respectively. A u-velocity profile through the cross section of this flow, passing through the center of the cavity's vortex, is shown in Fig. 11. This case typically illustrates results for cavities with the dividing streamline separating and reattaching within the cavity. These stagnation points can be located from the vorticity plots by looking for the locations along the vertical walls where the vorticity function is zero (i.e., changes sign). For comparison, another case is presented, in which the dividing streamline separates and reattaches slightly outside of the cavity. This cavity, with $\mathcal{R} = 0.67$, $Re_c = 8$ and

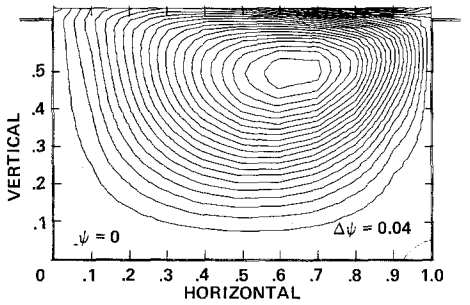

FIG. 12. Stream function contour map for the interactive shear layer–cavity solution: $\mathcal{R} = 0.667$, $Re_c = 8.0$, $Re_{BL} = 10^5$, $Pr = 1$, $M_\infty = 2.25$.

$Re_{BL} = 10^5$, has the same depth but a 50% longer span than the other cases presented. The stream function map corresponding to this case appears in Fig. 12.

The run-time for the typical case of 12 boundary layer steps per sweep with the Navier–Stokes field of 11×25 grid points (corresponding to $AR = 1$ cavity), allowing for 20 sweeps and the initial calculation of the boundary layer, was about four minutes on IBM 370-168 computer, and about 50 sec on a CDC 7600.

Discussion of Results and Evaluation of the Method

The examination of the effect of reduction of grid spacing in Fig. 5 indicates that the grid size used in the computation of remainder of the results presented was sufficiently small. The only distinguishable difference is seen to be the resolution of the additional, highest value, streamline in the center of the vortex computed with the fine grid. Although indistinguishable in the plotted results, the location of the stagnation points did show a slight shift of about $0.1\,\Delta y$.

Comparison of the results for shear layer driven cavity with those where moving wall was used (Fig. 6) not surprisingly show considerable discrepancy in the upper part of the flow. It is also seen that the mass inflow between the upper upstream corner and the streamline above is a controlling parameter affecting the recirculatory flow solution. However, even when the mass influx is held fixed (compare Data 10 with Data 12), there is some sensitivity of the secondary flow to the actual distribution of driving velocities along the interphase.

The location of the stagnation points of the dividing streamline is determined routinely by the Navier–Stokes formulation for recirculating flow, as was illustrated in Figs. 7 and 8. The method is also capable of handling cases where the dividing streamline stagnates outside the cavity region, such as in the case of a 50% longer cavity in Fig. 12. Since the stagnation points for this case fell within one grid point of the cavity, no adjustment of the Navier–Stokes region was needed. However, should the dividing streamline fall outside the region where the elliptic equations are solved, this region can be readjusted in size to contain fully the dividing streamline. This capability of the present method of routinely treating the stagnation points enhances its usefulness and is considered worthy of emphasis.

The two-boundary matching method proved to be most satisfactory. This is seen by examining the graphs of the u and v components of velocity in the matching region shown in Figs. 9 and 10. Both u and v are successfully matched (identical values of the variables computed by the Navier–Stokes and boundary layer equations) along the lower matching line. Along the upper matching line, u velocity is matched to within fraction of one percent, but v shows a somewhat more significant mismatch. Thus it is concluded that both u and v are matched along cavity's upper boundary, with $\partial u/\partial y$ also matched along that boundary. This continuity of the u velocity profile is clearly seen in Fig. 11. Furthermore, mass was conserved along the cavity's upper boundary. These statements hold for all cases examined.

The wiggle in the v-velocity distributions along the matching line which appears at the upstream extreme in Fig. 10 was also found to be recurring in other cases. Its severity was found to be directly related to the magnitude of v, and its cause is attributed to the step-like change in the velocities at the cavity's leading edge arising from neglecting the upstream influence (i.e., dp/dx) in the present model.

Conclusions

A new interactive method was presented for computation of flow fields consisting of regions in which parabolic and elliptic mathematical models are used. Application was made to the shear layer driven cavity flow.

The method was shown capable of yielding uniform solutions to the flow fields considered, by successfully matching the flow variables u, v, and $\partial u/\partial y$ along the cavity shear layer interface. The stagnation points presented no special problem, and their location was determined from the iterative solution and was not specified a priori. The computation time required for a converged solution was modest.

Comparison of solution for the shear layer driven cavity with the corresponding case of cavity driven by a moving wall showed that proper mass influx is an essential factor in the reversed flow solution. It is inherent in the method presented in this paper, but is lacking if an approximation is used for driving the recirculating flow solution.

Currently, the present method is being used for investigation of several aspects of shear layer driven cavity flows.

References

1. C. J. Borland, AIAA Paper 77–673 (1977).
2. J. Brandeis, D.Sc. thesis, Technion–Israel Inst. of Tech. (1979).
3. D. R. Chapman, NASA Rep. 958 (1950).
4. A. F. Charwat, J. N. Roos, F. C. Dewey, Jr., and J. A. Hitz, *J. Aero. Sci.* **28** (1961), 457.
5. A. F. Charwat, F. C. Dewey, Jr., J. N. Roos, and J. A. Hitz, *J. Aero. Sci.* **28** (1961), 513.
6. U. B. Mehta and Z. Lavan, NASA CR-1245 (1969).
7. V. O'Brien, *Phys. Fluids* **15** (1972), 2089.
8. T. A. Reyhner and I. Flugge-Lotz, *Int. J. Non-Linear Mech.* **3** (1968), 173.
9. P. J. Roache, "Computational Fluid Dynamics," Hermosa, Albuquerque, N.M., 1972.
10. J. Rom, *SIAM J. Appl. Math.* **29** (1975), 309.
11. R. F. Weiss and B. H. Florsheim, *Phys. Fluids* **8** (1965), 1631.